ORIGINAL ARTICLE

An adaptive neuro-fuzzy and NSGA-II-based hybrid approach for modelling and multi-objective optimization of WEDM quality characteristics during machining titanium alloy

Ashish Goyal[1] · Nipun Gautam[1] · Vimal Kumar Pathak[1]

Abstract

In this paper, an intelligent approach of adaptive neuro-fuzzy inference system (ANFIS) and non-dominated sorting genetic algorithm-II (NSGA-II) was delineated to establish model and optimize the wire electrical discharge machining (WEDM) process. The WEDM experiments were designed utilizing Taguchi L18 mixed orthogonal array for machining of Ti–6Al–4V titanium alloy. The ANFIS model was delineated to explain the influence of input machining characteristics, viz. peak current (IP), pulse on-time (T_{on}), pulse off-time (T_{off}) and wire feed (WF) on output response of material removal rate (MRR) and wire wear ratio (WWR). The proximity of results with confirmation experimental results revealed the effectiveness of the developed ANFIS model in prediction of output quality characteristics for the chosen input machining factors. The artificial neural network (ANN) and NSGA-II were integrated and applied for multi-objective optimization in determining optimal WEDM machining process conditions. The optimal results obtained with NSGA-II for multi-objective optimization of input control variables are within tolerance limits and realized an improvement in MRR and WWR (maximum absolute percentage errors as 6.784% and 7.589%) with optimal machining characteristics.

Keywords WEDM · ANFIS model · MRR · WWR · NSGA-II · Titanium alloy

1 Introduction

From the last decade, the use of Ti–6Al–4V titanium alloy, also known as Ti64, has increased considerably for the manufacturing of important automotive, aircraft and biomedical parts owing to its higher strength-to-weight ratio, high fracture toughness, better corrosion resistance and good biocompatible properties [1–3]. However, such superior characteristics and poor machinability of the titanium alloy result in higher friction, excessive heat generation and built-up-edge formation with traditional machining processes. Therefore, these alloy materials are sometimes known as difficult-to-cut materials in the context of machining in the literature [4, 5]. In the present scenario, the possible solutions for effective machining and overcoming the challenges imposed by difficult-to-cut materials can be realized by non-traditional machining processes. The wire electrical discharge machining (WEDM) is a well-known abrasion less non-traditional machining processes, which can machine hard surfaces with ample ease and can achieve high quality complex surfaces with the help of consuming wire electrodes [6]. The WEDM is a contactless process of thermo-electrical machining that perform material removal by spark erosion and vaporization of material in between workpiece and the wire electrode. However, the selection of optimal machining parameters is one of the important and challenging tasks for the industrial personnel, operators and users that further influence the performance of EDM machining process [7].

The WEDM material removal process performance is significantly affected by direct and indirect control factors such as peak current, gap voltage, pulse on-time, pulse off-time, wire feed and mechanical properties of wire and workpiece material. Several studies are available for determining effect of input machining parameters in

✉ Vimal Kumar Pathak
vimalkumar.pathak@jaipur.manipal.edu

[1] Department of Mechanical Engineering, Manipal University Jaipur, Jaipur, Rajasthan 303007, India

WEDM on the optimal quality characteristics of kerf width, surface roughness and material removal rate (MRR). The application of Taguchi orthogonal array for planning of experiments were studied by different researchers during the machining of Inconel 625 and aluminium alloy examining the influence of pulse on-time, pulse off-time, peak current, wire feed rate and wire tension on MRR and surface roughness. It was concluded that the pulse on-time, tool electrode and current intensity has an imperative effect on the responses of MRR and surface roughness [8, 9]. Kuriachen et al. applied fuzzy logic-based model for examining the effect of different process parameters such as gap voltage, capacitance, feed rate and wire tension for prediction of MRR and surface roughness during EDM of titanium alloy [10]. The non-dominated sorting genetic algorithm-II (NSGA-II) with Pareto optimal solutions was applied for the optimization of the MRR and surface roughness in machining shape memory alloys and tungsten carbide–cobalt composite [2, 3]. Manna and Bhattacharyya applied Taguchi experimental design and the Gauss elimination dual response method for determining the optimum machining process conditions during CNC WEDM of aluminium reinforced silicon carbide metal matrix composites [11].

Bobili et al. used Buckingham Pi theorem to evaluate the influence of input machining characteristics on MRR and surface roughness for WEDM of two different armour materials like aluminium alloy 7017 and RHA steel. The results revealed that with higher value of pulse on-time, both the output response of MRR and surface roughness improve during machining [12]. Majumdar in his study applied hybrid approach of fuzzy logic and particle swarm optimization (PSO) and investigated the influence of pulse current, pulse on-time and pulse off-time on MRR and EWR during machining of AISI 316 LN stainless steel [13]. The advantage of multiple regression and Taguchi analysis for predicting MRR and surface roughness in EDM was studied and results are further optimized using GA for determining optimal set of input parameters for higher MRR and minimum surface roughness [14, 15]. In other study, Goswami and Kumar used Taguchi planned experiments on EDM for investigating the MRR, surface integrity and wire wear ratio of Nimonic 80A. The results revealed that pulse on-time and peak current increases the recast layer thickness, while the pulse on-time and pulse off-time significantly affect the MRR [16]. Further, machining of high-strength low-alloy (HSLA) steel studied the effects of various process variables using RSM and GA methods on the overcut value [6]. Similarly, the influence of different EDM process parameters on surface roughness and MRR was determined during machining of hard Inconel 600 alloy and AISI D2 steel workpieces. It was revealed from both studies that current intensity and pulse on-time are most influencing factors for achieving optimal values of output responses [17, 18]. Kumar et al. applied grey relational analysis to optimize kerf width and surface roughness during WEDM of hard silicon carbide reinforced aluminium 6351 alloy composite. They recommended that pulse on-time was most effective in influencing the combined objective with 96.19 percentage [19]. In a similar study, Yang et al. explored hybrid methodology of RSM, BP neural network and simulated annealing (SA) for optimizing three different objective functions, viz. MRR, surface roughness and corner quality during machining of tungsten workpiece. They found that the integration of BPNN and SA provides superior results in comparison to RSM approach results [20].

From the literature review, it was revealed that modelling a mathematical correlation equation between input control variables and the output response quality parameters is exceedingly strenuous in WEDM owing to its intricate and non-sequential nature of these machining parameters [21]. The development of a complex modelling system is essential for predicting and optimizing the quality characteristics as responses for a given set of process parameters that further decreases the production cost. In relation to WEDM process, most of the modelling has been performed using the traditional optimization techniques. Several research work presented in past employed ELMAN-based layer recurrent neural network (LRNN) [22], artificial neural network (ANN) combined with a genetic algorithm (GA) [23], regression model and feed forward backpropagation neural network [24], backpropagation neural network (BPNN) and response surface methodology (RSM) [25], grey fuzzy logic [26] and BPNN approach [27] for machining different workpiece using WEDM.

Based on the past literature results, it is observed that none of the research reported developing a hybrid approach for modelling the output quality characteristics by incorporating the advantages of both fuzzy and ANN for WEDM of Ti–6Al–4V alloy. The wire wear ratio (WWR) is a critical response parameter which was not considered in past studies for modelling of WEDM process during machining of titanium alloys. In addition, the machining ability of brass wire electrode in WEDM and prediction accuracy of developed model hybrid model were not critically evaluated in most of the studies. Finally, very few studies are available that performs optimization of quality characteristics using NSGA-II for WEDM of titanium alloys.

Therefore, the objective of present work is to conduct a logical investigation while machining titanium Ti–6Al–4V alloy employing WEDM process and to establish an effective adaptive network-based fuzzy inference system (ANFIS) prediction model to improve the machining

characteristics, i.e. material removal rate and wire wear ratio. Moreover, the results of ANFIS-based prediction model are compared with experimental results in terms of accuracy and root mean square error percentage. The machining parameters of WEDM were optimized by applying non-dominated sorting genetic algorithm-II (NSGA-II) and optimal set of input control parameters were determined. The proposed methodology of combining ANFIS model and NSGA-II will be beneficial in optimal modelling and prediction of input process parameters for the manufacturing of components in different industries.

2 Experimental details

2.1 Workpiece material

The workpiece material used in this study is α–β titanium (Ti–6Al–4V) alloy with dimensions of 150 mm $\times$ 50 mm $\times$ 3 mm was prepared. The titanium alloy is selected owing to its higher strength-to-weight ratio and supreme resistance towards corrosion making it suitable candidate for aerospace and automotive applications. The chemical composition of Ti–6Al–4V alloy using an energy-dispersive X-ray (EDX) (Quanta 450 FE-SEM, FEI), which is shown in Table 1. The rectangular slots of 3 mm $\times$ 3 mm were machined from 3-mm-thick alloy plate specimen at different set of machining conditions. The fabricated specimen after machining at various parameter settings is shown in Fig. 1.

2.2 Experimental set-up

The current section describes the EDM equipment employed for performing the planned experiments, with the material used for workpiece along with the brief description of ANFIS and NSGA-II methodology. The planned experimental trials were conducted on WEDM machine (Sprint-Cut 734, Electronica, India) with a jet flushing system at a pressure of 50 kPa. A brass wire (65% Cu and 35% Zn) is used as a tool electrode for the present work with diameter of 0.25 mm. The dielectric fluid considered for the experiments is mineral oil having flash point of 72 °C. The experimental set-up for the present study is shown in Fig. 2. Since the output quality characteristics in WEDM is affected by different process variables, this study deals with considering the influence of electrical process parameters, viz. peak current (I_P), pulse on-time
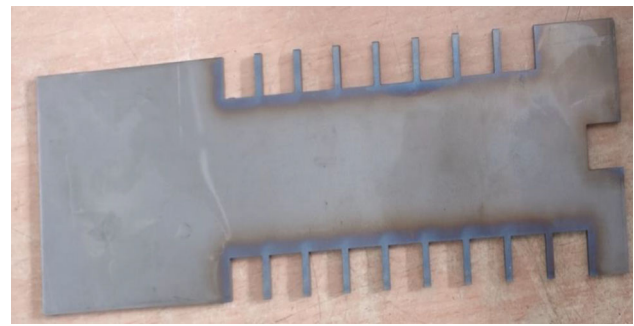

Fig. 1 Machined Ti–6A1–4V alloy specimen with slots

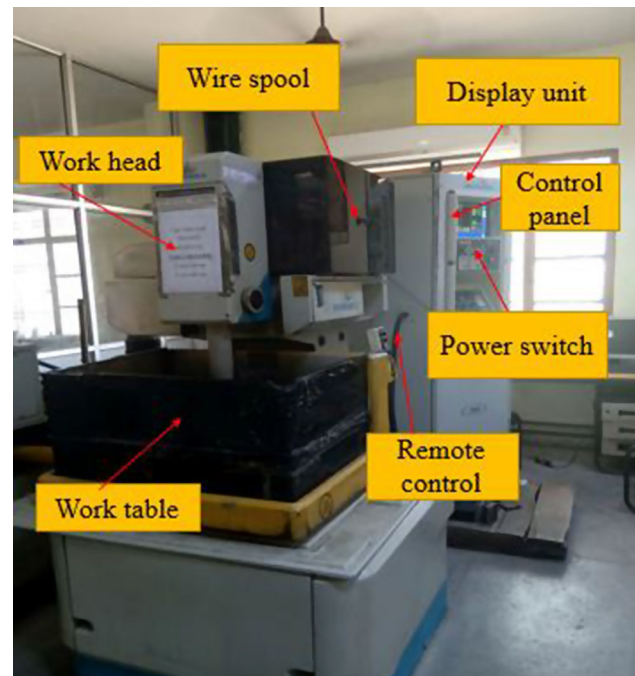**Fig. 2** Electronica Sprint-Cut 734 EDM machine

(T_{on}), pulse off-time (T_{off}), wire feed rate (W_f) of the WEDM operation on the output response of material removal rate and wire wear ratio. The input variables with their levels are selected on the basis of the literature, trials and machine constraints are shown in Table 2.

The peak current, pulse on-time, pulse off-time and wire feed rate have been selected as input parameters, and the effect of these input parameters has been investigated on material removal rate and wire wear ratio. The peak current is the maximum current of each pulse applied between both the electrodes when the spark is created. The pulse on-time and pulse off-time, measured in microseconds, are the duration for which current is flowing till end of discharge

Table 1 Chemical composition of workpiece (Ti–6Al–4V) alloy [28]

Component	C	Sn	Si	Mn	Fe	Cr	Ti	Al	V
Weight %	0.006	0.001	0.01	0.0053	0.091	0.021	89.83	6.321	3.714

Table 2 Process parameters and their levels

Parameter	Symbol	Unit	Level 1	Level 2	Level 3
Peak current (A)	IP	Ampere	16	22	–
Pulse on-time (B)	T_{on}	μs	120	140	160
Pulse off-time (C)	T_{off}	μs	35	40	45
Wire feed (D)	W_F	Machine unit	6	8	10

and the duration between two consecutive pulses, respectively. The wire feed is the advancement of wire electrode in machining direction with the help of servo motor per minute. The material removal rate was measured in mm³/min by using Eq. (1):

$$\text{MRR} = \frac{d \times l \times h}{t} \ \text{mm}^3/\text{min} \tag{1}$$

where t is the machining time, h is the height of the workpiece, l is the length of the cut and d is the kerf width. MRR was calculated in mm³/min. The weight of the removed wire is measured by the weighing machine, Sartorius, model: BSA225S-CW. The wire wear ratio is measured using Eq. (2).

$$\text{Wire wear ratio} = \frac{\text{Initial weight of wire} - \text{Final weight of wire}}{\text{Initial weight of wire}} \tag{2}$$

2.3 Taguchi experimental design

In present study, the experiments were performed to determine and optimize MRR and WWR using Taguchi orthogonal array design. The Taguchi technique provides a platform for statistical and mathematical models to optimize the response variables. The Taguchi method procedure allows a synchronized experimental trial of different parameters and their interaction effects planned for evaluating the consequence of the parameters on response variables [29]. In traditional full factorial design, it needs $3^4 = 81$ experimental trials to study and analyse four input factors. However, in the present work Taguchi experimental design suppresses it to only 18 trials using L_{18} $(2^1 \times 3^4)$ mixed orthogonal array, thus reducing the number of experiments significantly and saving precious time and the cost associated with it. The data assembled from experimental results are then transformed to calculate signal-to-noise (S/N) ratio. The S/N ratio is the performance indicator of output response and is chosen based on certain quality characteristics such as lower-is-better, nominal-is-better and higher-is-better. This work aims at maximizing MRR and minimizing the WWR; thus, higher-is-better and lower-is-better characteristics are chosen to evaluate the S/N ratio performance and can be expressed as shown in Eq. (3) [30]:

$$\frac{S}{N} = -10\log\left[\frac{1}{n}\sum_{i=1}^{n} y_i^2\right] \tag{3}$$

where y_i represents the response of specific wear rate and n denotes the number of experimental trials. Table 3 shows the experimental conditions and measured responses based on Taguchi L18 mixed orthogonal array. The minimum and maximum values of MRR and WWR for the machined specimen are 19.11–9.92 mm³/min and 0.371–0.057, respectively. Table 3 reports 18 experimental data that were selected for testing of adaptive neuro-fuzzy inference system (ANFIS) and random 50 experiments samples are utilized for testing the accuracy of the trained ANFIS model.

### 2.4 Adaptive neuro-fuzzy inference system (ANFIS)

The ANFIS network generally refers to adaptive neuro-fuzzy system inheriting the advantages of both fuzzy network and artificial neural network [31]. Neural network can enhance the learning process; however, it is quite difficult to deduce the data and knowledge acquired by it. Instead, the fuzzy logic system cannot learn itself from the samples but utilizes the linguistic variables as crisp set values in place of numeric values which are easy to comprehend and follow. In ANFIS network, the ANN architecture is employed to develop the fuzzy model and through which it aids in learning the ANN data from the given data. Simultaneously, the results are plotted for different factors arranged in Sugeno category of if–then rules. The schematic diagram of ANFIS architecture is shown in Fig. 3. As shown in Fig. 3, five different layers are utilized to develop the ANFIS network. The procedure of ANFIS modelling begins with converting the crisp input parameters into fuzzy inputs exploiting the membership functions.

From the commonly used membership functions such as triangular, trapezoidal and Gaussian, this study employs Gaussian and G-bell membership function in ANFIS model for assessment of input variables and triangular-type functions were chosen for output variables. Further steps deal with providing the Gaussian membership functions along with fuzzy input to the neural network. The back-propagation algorithm is applied to train the inference engine for appropriate rule base selection in the neural

Table 3 Experimental trials and response results

Ex. No.	Peak current (A)	T_{on} (μs)	T_{off} (μs)	Wire feed (m/min)	MRR (mm³/min)	WWR
1	16	120	35	6	12.56	0.068
2	16	120	40	8	11.86	0.082
3	16	120	45	10	9.92	0.057
4	16	140	35	6	12.09	0.062
5	16	140	40	8	16.76	0.094
6	16	140	45	10	13.43	0.06
7	16	160	35	8	18.08	0.1
8	16	160	40	10	13.81	0.088
9	16	160	45	6	16.12	0.074
10	22	120	35	10	10.51	0.108
11	22	120	40	6	11.11	0.128
12	22	120	45	8	12.89	0.114
13	22	140	35	8	17.06	0.242
14	22	140	40	10	15.47	0.2
15	22	140	45	6	15.85	0.157
16	22	160	35	10	19.11	0.371
17	22	160	40	6	17.22	0.314
18	22	160	45	8	18.20	0.214

Fig. 3 Schematic of ANFIS architecture
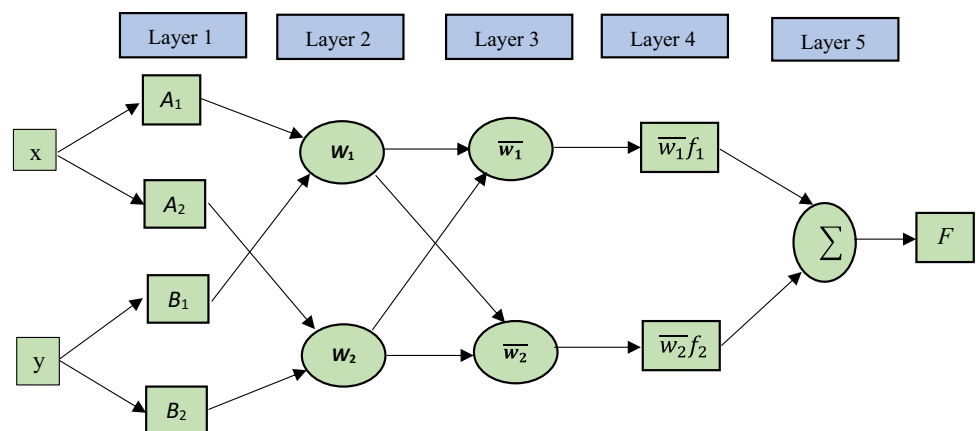
network block. After adequate training, suitable rules are fired from the neural network to produce the optimal output. Finally, the output variable in linguistic terms is converted into crisp output by the de-fuzzifier block. The structure of ANFIS based on Takagi–Sugeno system comprises of five different network layers, i.e. Layer 1 to Layer 5. For describing the ANFIS procedure, two inputs x and y, one output F. The Takagi–Sugeno ANFIS rules base consists of if–then fuzzy rules and that can be expressed as:

Rule 1: If x is A_1 and y is B_1, then output is $f_1 = a_1 x + b_1 y + c_1$

Rule 2: If x is A_2 and y is B_2, then output is $f_2 = a_2 x + b_2 y + c_2$

2.4.1 Layer 1

The first layer deals with conversion of set of inputs (x, y) into linguistic terms $(A_1, A_2, B_1$ and $B_2)$ by applying membership function. Fuzzy layer comprises of set of adaptive nodes whose function is expressed as Eqs. (4)–(5):

$$O_{1,i} = \mu A_i(x) \quad \text{for } i = 1, 2 \tag{4}$$

$$O_{1,i} = \mu B_{i-2}(y) \quad \text{for } i = 3, 4 \tag{5}$$

where $O_{1,i}$ represents the output function. μA_i and μB_{i-2} represent the membership functions. For the present study, Gaussian membership function is selected for input and triangular membership function is chosen for output.

2.4.2 Layer 2

The second layer shown with circle deals with obtaining the output signal by multiplying the input signal received from previous layers with fixed node function denoted as $O_{2,i}$. The output of every node provides the firing strength of a rule as expressed in Eq. (6).

$$O_{2,i} = w_i \mu A_i(x) \mu B_i(y) \quad \text{for} \quad i = 1, 2 \tag{6}$$

2.4.3 Layer 3

The third layer, also named as normalized layer, is represented in Eq. (7) as ratio of individual rule of firing strength to the algebraic sum of all the firing strength.

$$O_{3,i} = \bar{w} = \frac{w_i}{w_1 + w_2} \tag{7}$$

where $O_{3,i}$ and $\bar{w}$ represents the output of third layer and firing strength, respectively.

2.4.4 Layer 4

The fourth layer is also referred to as defuzzification layer where each node of layer is adjustable and variable in nature. The output node function can be represented as Eq. (8):

$$O_{4,i} = \bar{w}f_i = \bar{w}(a_i x + b_i y + c_i) \tag{8}$$

where a_i, b_i and c_i are the set of consequent parameters for rule i.

2.4.5 Layer 5

The fifth layer shown by circle consist of only one node. It evaluates the overall ANFIS output by summing up the all the output coming from previous layer and can be expressed as Eq. (9):

$$O_{5,i} = F = \sum_i^2 \bar{w}f_i \tag{9}$$

2.5 Non-dominated sorting genetic algorithm-II (NSGA-II)

This study employed NSGA-II for optimizing the complex and conflicting objective functions, i.e. MRR maximizing and WWR minimizing, in WEDM process. In contrast to single-objective functions where only one optimal solution exists, the multi-objective functions consist of more than one solution. Numerous traditional techniques are available in the literature for solving multi-objective functions; however, they suffer from shortcomings such as weighting

the objectives having more relevance; thus, the user must have adequate knowledge of all the objective functions considered. Moreover, no such requirement needed in NSGA-II algorithm and it is free from gradient requirements during finding the solution in search space. The NSGA-II algorithm is primarily based on Pareto optimal set and effective in finding the optimal solution for non-trivial real life multi-objective problems [32]. Beginning with generation of initial population of size n using ANFIS model, subsequently the comparison of different solutions takes place for determining the set of optimal solutions. The solution under consideration must satisfy the following rules for non-dominated sorting.

Objective $1[i] >$ Objective $1[j]$ and
Objective $2[i] \geq$ Objective $2[j]$
Or
Objective $1[i] \geq$ Objective $1[j]$ and
Objective $2[i] >$ Objective $2[j]$

where $i \neq j$, and they are referred as solution numbers.

For sorting of n non-dominated solutions, solution was chosen based on justifying the above criteria and are assigned rank 1; otherwise, solutions are marked as dominated solutions. Similarly, next non-dominating sorting takes place from dominated solution and assigned rank 2 and so on. These iterations will be continued till all solutions received their rankings. Further, based on their ranking fitness value is assigned to each of the solutions. The crowding distance (CD) is evaluated for each of the non-dominated solutions and higher value of CD provides better diversity among population. The comparison between tournament choice and CD was utilized for the selection of parents. The offspring generated using mutation and crossover operator, and initial population along with offspring were used for realizing the non-dominated solution. This solution was selected if the newly generated population exceeds maximum solution; else, new population was generated followed by the above steps until Pareto front of non-dominated result is found. For more reading on NSGA-II, researchers can go through the following studies [33].

3 Result and discussion

This section comprises of three main parts: the first part deals with development of predictive model based on ANFIS. The second part deals with the description about influence of EDM process parameters on the response variables (MRR and WWR) using surface plots obtained from developed ANFIS models. At last, the third part

involves simultaneous optimization of EDM response variables using NSGA-II.

3.1 Development of ANFIS model

The ANFIS structure and model are developed utilizing MATLAB ANFIS editor toolbox for predicting separately MRR and WWR for the EDM machined titanium alloy. It exploits the Sugeno-based fuzzy inference system and the membership functions are used to perform training of the model and for mapping relationship between process inputs and the response variables. The prediction of MRR and WWR of the EDM using ANFIS model involves two main steps: training and testing. Therefore, fifty randomly performed experimental datasets have been selected for training and sixteen sample data of Table 3 for testing process. The testing datasets are selected, and testing of the ANFIS model was performed that have not contributed to training process. The accurate prediction of results using ANFIS structure depends on some important parameters such as number of membership function, number of iterations and type of membership function. In the same context, during the training process of designed ANFIS model, the input data were plotted several times to reduce the error. The number of iterations for adequate mapping is considered as epochs. In order to further improve the results of ANFIS model, different types of membership functions were employed, and root mean square error (RMSE) is measured and compared. Training epochs are continued till it reaches an assumed value say 400 or fall below a specified value (0.005) of RMSE.

The best membership function is selected based on low value of RMSE in the training phase having accurate prediction of new input data when compared with experimental values. After testing various models of ANFIS structure separately for each of the two responses (MRR and WWR), it was resulted that model structure with 12 membership function (3–3–3–3 topography or 3 membership function for each response) has the lowest value of RMSE. Other structures with lower and higher membership functions resulted in either underfitting or overfitting with undesired values of error. The model and structure of developed ANFIS model for MRR and WWR is shown in Figs. 4 and 5. Other factors affecting the prediction accuracy of ANFIS structure is type of membership function. For this study, six different membership functions available in ANFIS editor were tried, and selection was performed based on the lower RMSE value. For this study, Gaussian membership function was employed for the assessment of input variables and triangular-type functions are chosen for output variables as shown in Fig. 6.

Table 4 shows the RMSEs results for different membership functions in testing of MRR and WWR. Table 4

shows that six different 3–3–3–3 structure membership functions were trained and tested, and the result shows that Gaussian membership function has the lowest value of RMSE and hence greater prediction accuracy for both material removal rate and wire wear ratio.

The comparison of experimental and predicted value of ANFIS model for MRR and WWR is presented in Table 5. The variation of predicted values (E_f) from actual measured experimental value (E_m) is used to calculate error percentage (E_p) after dividing the absolute difference between the above values by the measured experimental value as shown in Eq. (10).

$$E_p = \frac{(|E_f - E_m|)}{E_m} \times 100\% \tag{10}$$

Furthermore, the accuracy is calculated by determining the closeness of the predicted ANFIS model value to the measured experimental value. Equation (11) is used to calculate accuracy, where A_m is the accuracy of the model and n is the total number of considered samples for finding the average individual accuracy.

$$A_m = \frac{1}{n} \sum_{i=1}^{n} \left(1 - \frac{(|E_f - E_m|)}{E_m} \right) \times 100\% \tag{11}$$

The highest and lowest error percentage between measured and predicted ANFIS model results for MRR is 6.18 and 2.15, respectively. Similarly, the WWR highest and lowest error percentage between measured and predicted ANFIS model results is 8.77 and 2.27, respectively. The average percentage error for MRR and WWR is 5.35 and 5.13, respectively. Such a consistent and lower error percentage of the overall model specifies that the developed ANFIS model predicted the outcome which is in proximity with the experimental results. It is worth mentioning that the overall model accuracy comes out to be 94.76% in predicting the values of MRR and WWR in machining of titanium alloy through WEDM. Such a high overall model accuracy justifies the utilization of Gaussian ANFIS model for successful prediction of output responses in WEDM of titanium alloy specimen. Results in Table 5 clearly show that even though the levels of the individual input variables are different from the training values, the ANFIS model can predict the responses with an adequate accuracy level. The ANFIS model predicted values for MRR and WWR are in good proximity with the experimental measured values.
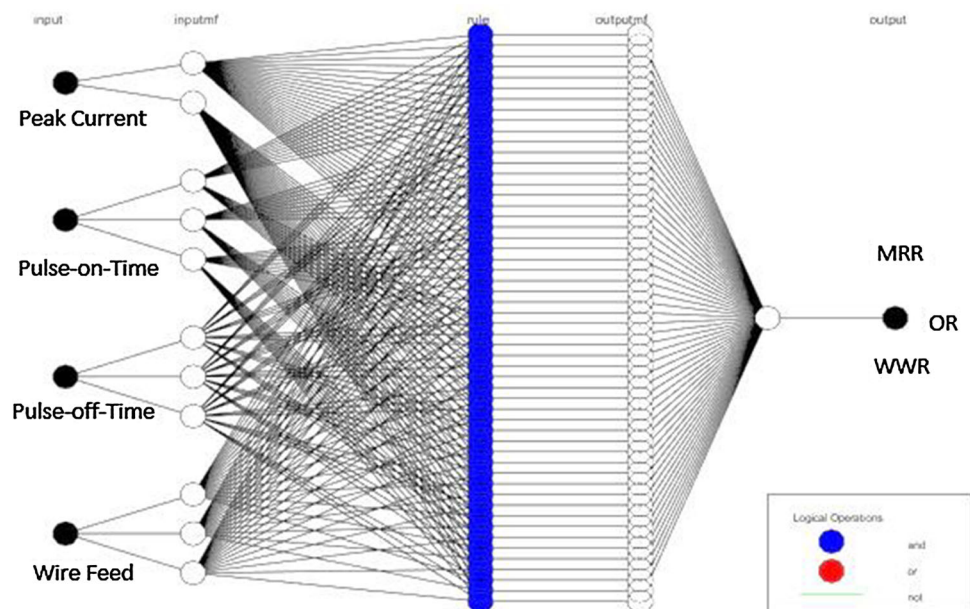
3.2 Analysis of responses

Here are the response surface analysis of material removal rate and wire wear ratio obtained through ANFIS models which are presented in Figs. 9 and 10, respectively. These

Fig. 4 Developed Sugeno ANFIS model
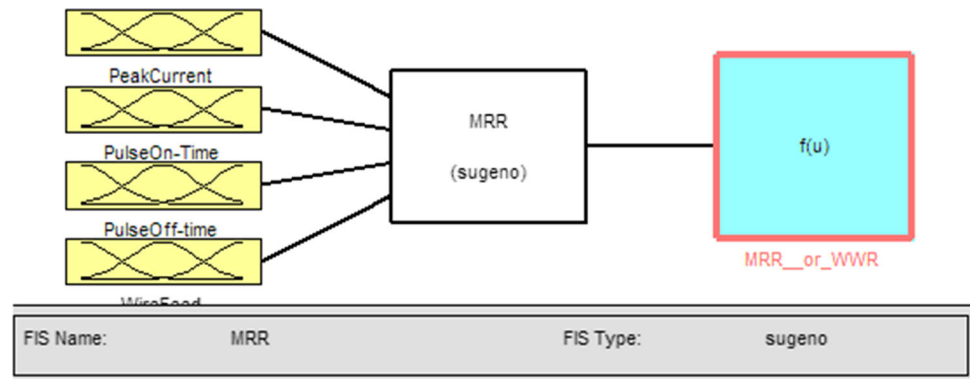
Fig. 5 Structure of the developed ANFIS model

3D surfaces show interaction effects between input parameters. Furthermore, these can be used for analysing effects input parameters on MRR and WWR as well.

3.2.1 Analysis of MRR

Figure 7a shows the interaction plot between pulse on-time and peak current. From this Figure, it was inferred that combination of high peak current and pulse on-time results in achieving higher value of material removal rate. The maximum MRR, i.e. 18 mm^3/min, was obtained at higher value of peak current and pulse on-time, i.e. 22 A and 160 μs, respectively. The possible reason may be attributed to the faster dielectric fluid ionization at higher value of current density, and hence, higher MRR is achieved. Figure 7b shows the surface plot that at 35 μs of pulse off-time and higher value of peak current more material removal rate is achieved. This may be due the higher value of Toff that provides proper flushing by dielectric medium to process. So, debris are removed properly form the

workpiece surface and more MRR is obtained. Figure 7c shows that combination of higher pulse on-time with medium to higher value of wire feed provides higher MRR primarily due to the increase in the discharge energy. Figure 7d, e shows that high and low value of wire feed improves the material removal rate due to less dissipation to the surrounding and more heat generated at spark gap, leading to more material melts from the workpiece surface, and higher MRR is gained. In Fig. 7f, the interaction plot between T_{on} and T_{off} shows that more material removal takes place at the higher value of T_{on} (140–160 μs) and T_{off} (45 μs). The higher value of thermal energy is generated that vaporizes and removes higher amount of material from sample surface. The increase in cutting time and the temperature of workpiece surface increase; thus, the more material is melted and MRR increases.
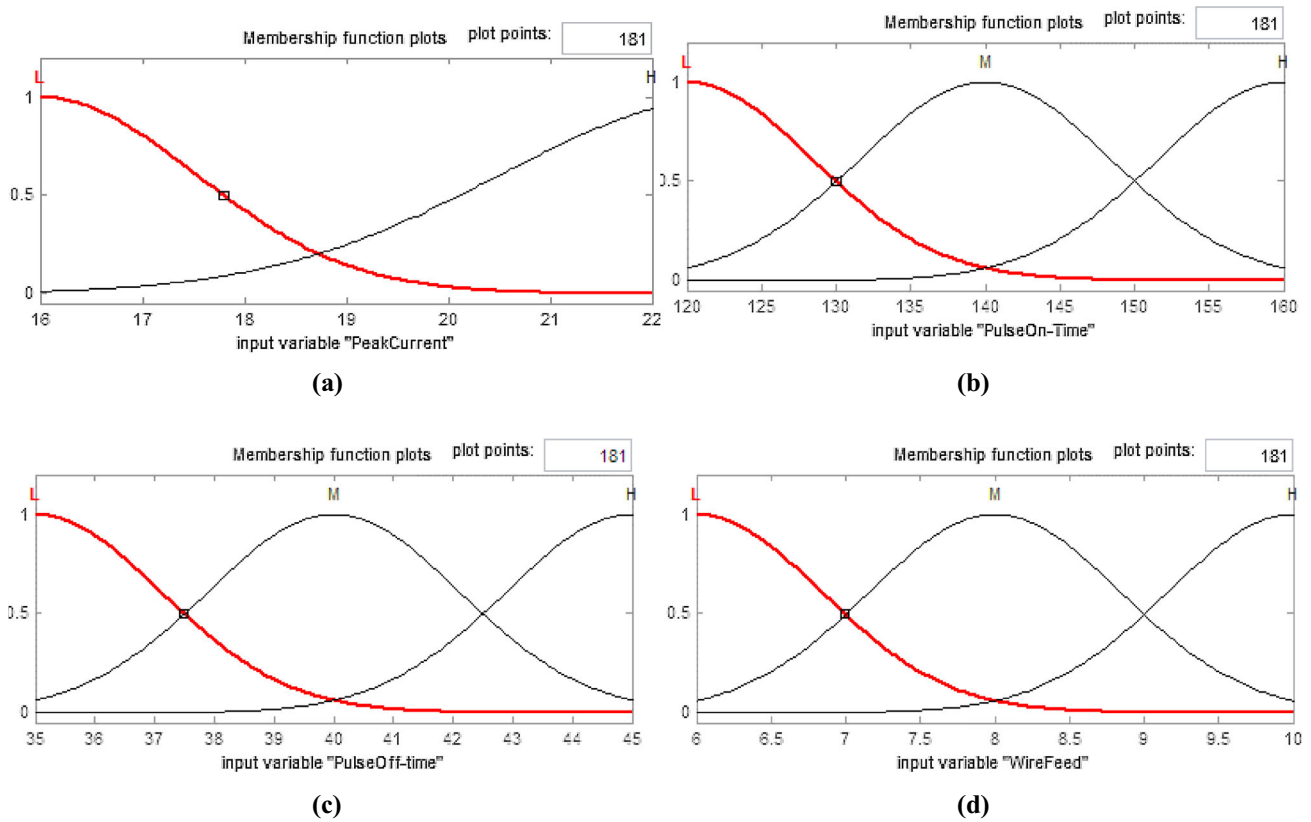
Fig. 6 Gaussian membership function for different input variables

Table 4 RMSE value for different membership functions

S. No.	Membership functions	RMSE of MRR	RMSE of WWR
1	Triangular	0.29630	0.55652
2	Trapezoid	0.26906	0.51773
3	G-bell	0.26044	0.51852
4	Gaussian	**0.23024**	**0.42451**
5	Pi shaped	0.28258	0.62924
6	D sigmoidal	0.29473	0.55392

Bold underline signifies the minimum RMSE value of membership functions

3.2.2 Analysis of WWR

Figure 8a illustrates the interaction plot between pulse on-time and peak current. From the figure, it was observed that low value of peak current, i.e. 16 A, combined with low pulse on-time around 120–140 μs provides low value of WWR, i.e. less than 0.06. This may be due to the lower value of discharge energy at low peak current and pulse on-time that save the wire electrode from wear out. Figure 8b, c shows that low tool wear ratio was achieved at medium value of pulse off-time, i.e. 40 μs, combining with low value of peak current. This may be because the proper flushing of the debris is performed and sticking tendency of debris to the tool surface decreases with the help of rotational movement of the workpiece and less wire wear ratio is achieved. Figure 8d shows the interaction plot for T_{on} and T_{off} and depicts that lower wire wear ratio can be obtained within a range of 35 to 40 μs values of pulse off-time and 120–140 μs for pulse on-time. This may be due to the combination of adequate machining time and enough time allowed for removing of debris from machining surface causing the minimization in sticking of wear debris on wire electrode and thus reducing the WWR value. Figure 8e shows prediction of WWR by varying pulse on-time and wire feed simultaneously. It was inferred that the moderate value of wire feed, i.e. 8 m/min, proved to be effective for minimizing the WWR. However, when wire feed rate was decreased from 8 to 6 m/min, higher value of wire wear rate is achieved. Figure 8f shows the interaction plot between wire feed and pulse off-time and predicts that higher pulse off-time leads to lesser WWR because of the reduction in the spark due to the removal of wear debris.

Table 5 Experimental and ANFIS predicted MRR and WWR

Ex. No.	Output parameters							
	Material removal rate (mm^3/min)				Wire wear ratio			
	Exp	Pred	Error %	Accuracy %	Exp	Pred	Error %	Accuracy %
1	12.56	11.50	8.44	91.56	0.068	0.07	2.94	98.06
2	11.86	11.50	3.03	96.97	0.082	0.078	4.88	95.12
3	9.92	10.50	5.84	94.16	0.057	0.062	8.77	91.23
4	12.09	13.05	6.95	93.05	0.062	0.064	3.22	96.78
5	16.76	15.92	5.01	94.99	0.094	0.090	4.25	95.75
6	13.43	14.05	4.61	95.39	0.06	0.063	5.00	95.00
7	18.08	16.45	9.00	91.00	0.1	0.092	8.00	92.00
8	13.81	14.35	3.91	96.09	0.088	0.086	2.27	97.73
9	16.12	16.00	0.74	99.26	0.074	0.081	9.45	90.55
10	10.51	11.50	9.41	90.59	0.108	0.113	4.62	95.38
11	11.11	11.50	3.51	96.49	0.128	0.122	4.69	95.31
12	12.89	12.40	3.80	96.2	0.114	0.118	3.51	96.49
	Average % error		5.35				5.13	

3.3 Parametric study using ANFIS model

3.3.1 Effect of peak current

Figure 9a shows that the MRR and WWR value increases with an increase in peak current. The MRR shows an uptrend from 10.56 to 18.10 mm^3/min with the increase in peak current owing to increase in the discharge energy. There is an enhancement in the duration of sparks as the peak current rises which assists in faster removal of material. Figure 9b shows that the WWR value increases from 0.877 to 0.0925 with the increase in the value of peak current from 16 to 22 A. The possible reason being higher peak current that develops concentrated thermal effect on the wire electrode causing its intense wear.

3.3.2 Effect of pulse on-time

Figure 10a clearly depicts that the value of MRR increases from 10.65 to 12.60 mm^3/min till the pulse on-time value reaches 145 μs and decreases further till 160 μs. The probable reason for such increase in MRR can be regarded due to the higher value of thermal energy with the increase in the pulse on-time that vaporizes and removes higher amount of material from sample surface. Figure 10b shows that as the pulse on-time was increased from 120 to 160 μs, the value of WWR increased gradually from 0.068 to 0.112. With higher pulse on-time, discharge energy rises causing an effective explosion, and hence, more electrode wear takes place.

3.3.3 Effect of pulse off-time

Figure 11a, b shows that the pulse off-time has negative influence on both MRR and WWR. The MRR decreases comprehensively with the increase in the pulse off-time value from 35 to 45 μs owing to decrement in the spark intensity. In contrast, the value of MRR is more when comparatively lower pulse off-time value is selected, providing higher spark intensity that melts and vaporizes more material. Similarly, Fig. 11b illustrates that with lesser pulse off-time, the discharge current is more, and thus, more material removal takes place which increases the WWR value.

3.3.4 Effect of wire feed

Figure 12a shows that with the increase in the value of wire feed from 6 to 10 machine units, the MRR value increased slightly from 9.95 to 10.14 mm^3/min owing to higher amount of material available at spark location, and thus, more discharge can be realized making material removal at more ease. Figure 12b provides insight into the influence of wire feed versus WWR. It is evident that with more material fed at spark location, the WWR value will increase due to enhanced wear of electrode wire.

3.4 NSGA-II-based optimization of WEDM

The prime objective of the current investigation is to maximize the MRR value and minimize the WWR. These objectives are of conflicting nature and are function of peak
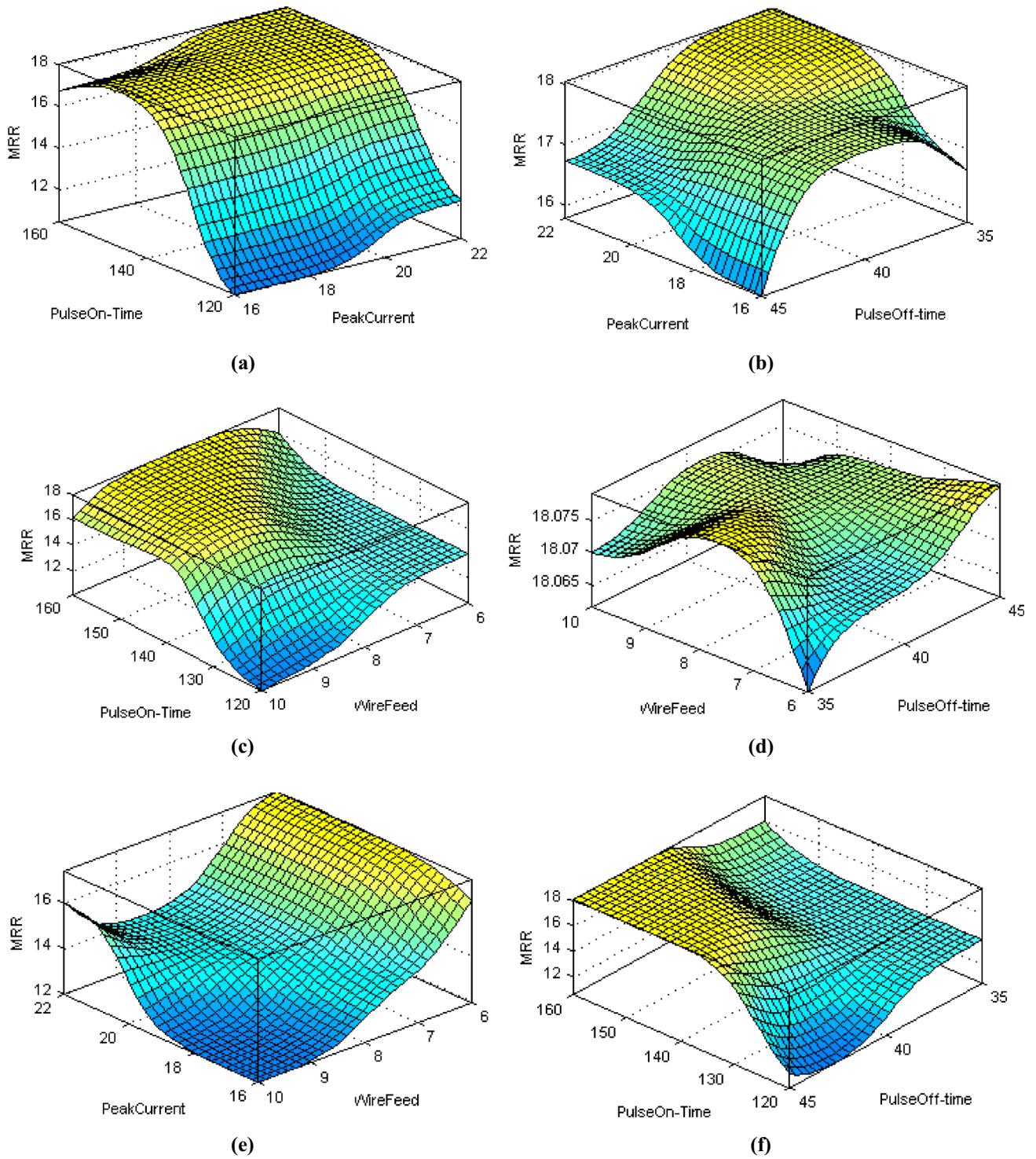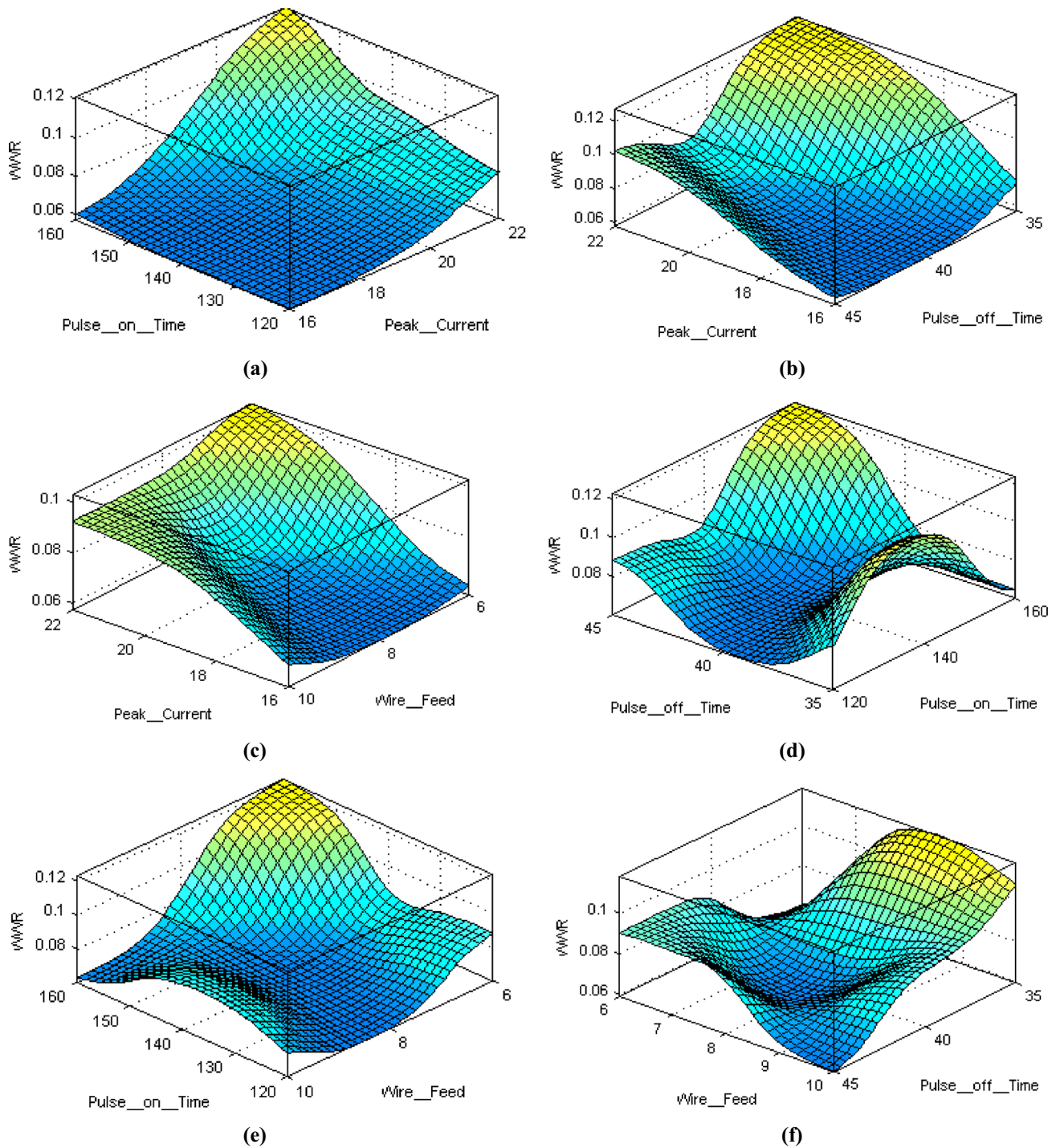
Fig. 7 a–f Surfaces plots of MRR by ANFIS

current (I_P), pulse on-time (T_{on}), pulse off-time (T_{off}) and wire feed rate (W_f). To solve the bi-objectives and avoid any conflict between two objectives, the objective of MRR is converted to minimization by adding negative sign as shown in Eq. (12).

Fig. 8 a–f Surface plots of WWR by ANFIS

Maximize MRR = Minimize(−MRR)
$$= F\left(I_{\mathrm{p}}, T_{\mathrm{on}}, T_{\mathrm{off}}, W_{\mathrm{f}}\right) \qquad (12)$$

and

Minimize WWR = $F\left(I_{\mathrm{p}}, T_{\mathrm{on}}, T_{\mathrm{off}}, W_{\mathrm{f}}\right)$

subject to constraints

$16 \leq I_{\mathrm{p}} \leq 22$
$120 \leq T_{\mathrm{on}} \leq 160$
$35 \leq T_{\mathrm{off}} \leq 45$
$6 \leq W_{\mathrm{f}} \leq 10$

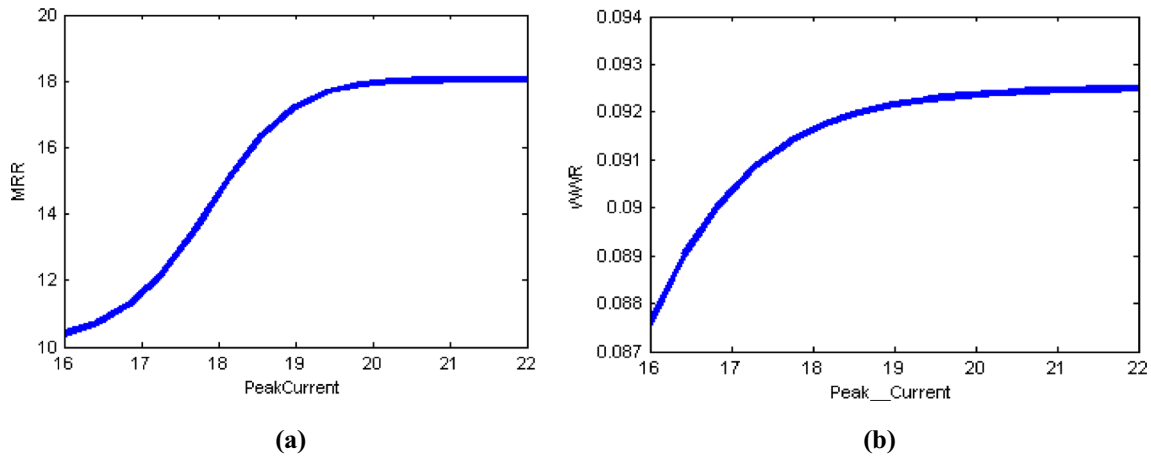For multi-objective optimization of input process parameters of WEDM, a hybridization of ANFIS output
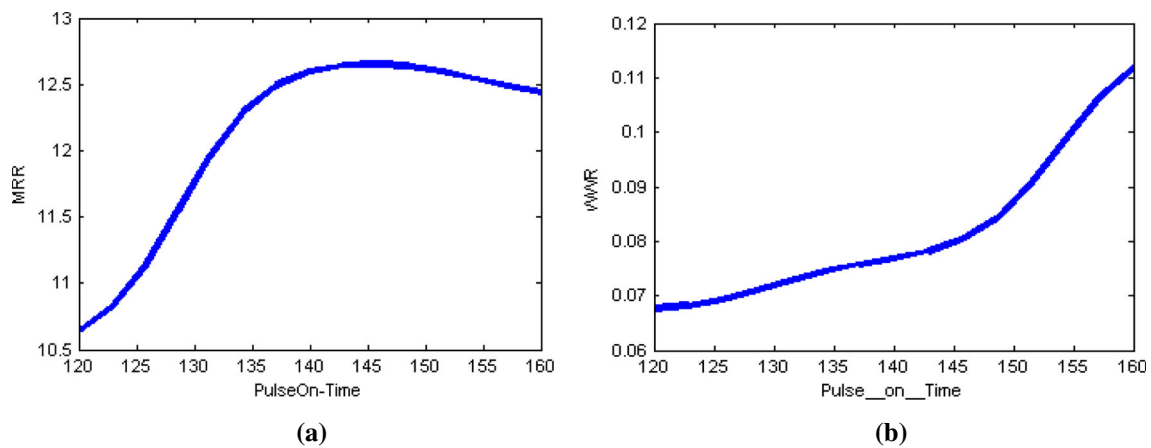
Fig. 9 Effect of peak current on **a** MRR, **b** WWR

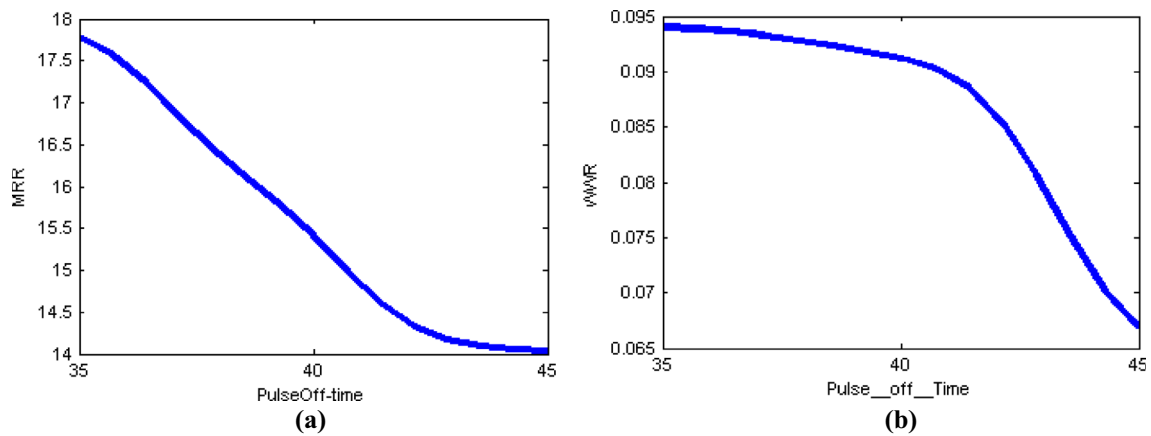**Fig. 10** Effect of pulse on-time on **a** MRR, **b** WWR

Fig. 11 Effect of pulse off-time on **a** MRR, **b** WWR

with NSGA-II is performed in MATLAB environment based on objectives and different constraints. The initial population generation takes place using ANFIS model in initial generations and further employed to evaluate the objective functions in subsequent iterations. For determining the non-dominated optimal results, different solutions are compared, while the best solution was chosen after the sorting and ranking performed by NSGA-II. The variable chosen for NSGA-II is based on the past literature and optimization problem for obtaining optimal solution
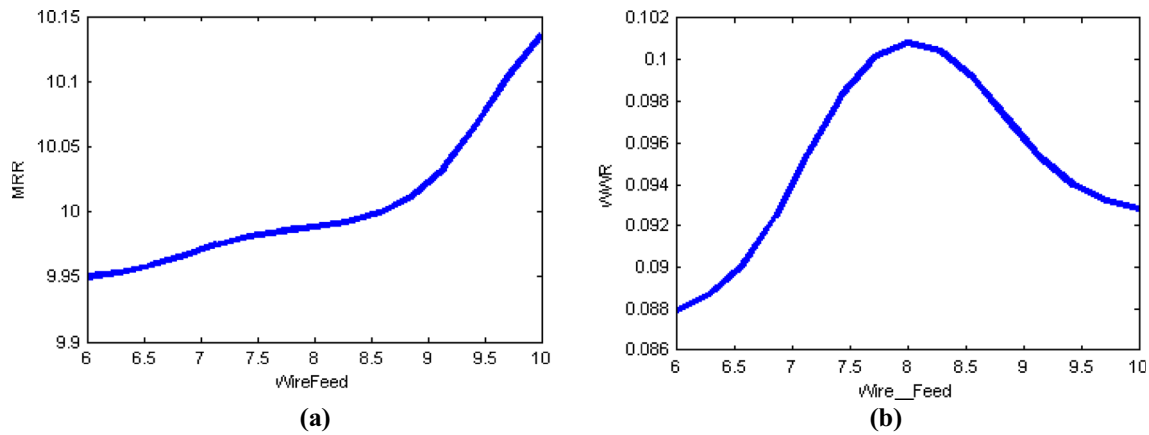
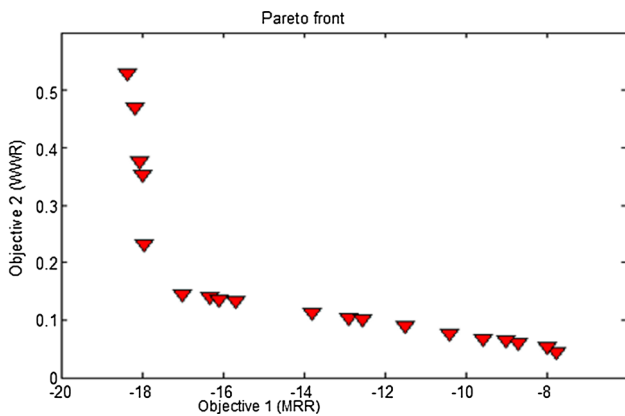Fig. 12 Effect of wire feed on **a** MRR, **b** WWR

Fig. 13 Pareto front of non-dominated solutions

with minimum computational cost. The population size considered for current study is 45 based on several experimental trials, which shows no appreciable change in objective function value after 45. The other important parameters considered for NSGA-II are selected as: maximum iterations = 100, mutation probability = 0.20 and crossover probability = 0.8. Figure 13 illustrates ultimate set of optimal solutions as the Pareto front of 23 results in

the exploration space for the optimization. The eight randomly selected optimal solutions out of 23 non-dominated solutions are reported in Table 6 and compared with literature results for WEDM using AHP-MOORA technique [34]. It was evident that the MRR and WWR value of proposed methodology is better (maximum for MRR and minimum for WWR) than literature technique.

3.4.1 Confirmation of optimal result

The proficiency of optimal response was examined by validation of the non-dominated solutions obtained using dual approach of ANFIS-NSGA-II with experimental trial results. The data of non-dominated solutions reported in Table 6 were considered and actual responses, i.e. MRR and WWR, obtained from experiments were reported employing the corresponding input WEDM parameters. Table 7 shows the comparison of experimental and optimal responses in the form of absolute error. From comparison, it was revealed that maximum absolute percentage errors value for MRR and WWR are 6.784% and 7.589%, respectively.

Table 6 Optimal combination of non-dominated solution for WEDM

S. No.	I_p	T_{on}	T_{off}	W_f	MRR	WWR	MRR [34]	WWR [34]
1	16.07	158.40	42.43	9.87	13.88	0.116	9.165	1.796
2	18.96	162.68	48.74	9.72	16.30	0.125		
3	17.87	159.82	48.12	10.25	16.95	0.143		
4	18.02	160.25	46.88	9.97	17.91	0.224		
5	14.38	155.33	40.25	9.08	11.62	0.094		
6	15.93	150.22	47.09	10.22	12.53	0.102		
7	18.51	160.79	48.02	9.98	18.10	0.348		
8	13.66	148.58	46.25	9.02	8.74	0.873		

Table 7 Comparison and validation of experimental and optimal responses of WEDM

S. No.	I_p	T_{on}	T_{off}	W_f	Optimal		Experimental		Absolute error	
					MRR	WWR	MRR	WWR	MRR	WWR
1	16	158	42	9	13.88	0.116	13.74	0.109	1.009	6.034
2	18	162	48	9	16.98	0.125	16.32	0.118	4.172	5.600
3	17	159	48	10	17.38	0.143	16.95	0.133	2.537	6.993
4	18	160	46	9	17.91	0.224	18.49	0.207	3.238	7.589
5	14	155	40	9	12.31	0.094	11.61	0.088	5.938	6.383
6	15	150	47	10	12.53	0.102	13.38	0.095	6.784	6.863
7	18	160	48	9	18.72	0.348	18.10	0.325	3.425	6.609
8	13	148	46	9.02	8.74	0.087	9.04	0.083	3.432	4.598

4 Conclusion

In this present study, a dual and intelligent approach of ANFIS–NSGA-II has been presented to minimize the WWR value and maximize the MRR during WEDM of titanium (Ti–6Al–4V) alloy. The experimental work consists of ANFIS modelling and multi-characteristic optimization of WEDM while machining Ti–6Al–4V alloy. The current, pulse on-time, pulse off-time and wire feed have been considered as input parameters. An adaptive neuro-fuzzy inference system was employed to create mapping relationship between process parameters and responses. Therefore, after the detailed study the following conclusions can be drawn:

- In modelling of MRR and WWR by ANFIS model, the 3–3–3–3 structure was chosen as the best topography due to its minimum prediction error and faster performance. The developed ANFIS model was found suitable to model the WEDM process during machining of titanium alloy.
- For ANFIS modelling, Gaussian type of membership function was utilized for MRR and WWR due to low value of RMSE. The developed ANFIS model predictions are in proximity with the experimental trials data and predict the MRR and WWR rationally well having average percentage errors as 5.35% and 5.13%, respectively.
- The ANFIS plot analysis revealed that with the increase in pulse on-time and peak current, the value of MRR and WWR increases significantly, while with the increase in the pulse off-time both MRR and WWR decrease comprehensively.
- The MRR and WWR decrease with the increase in the pulse off-time. The optimum settings of Peak current and pulse on-time were near to 18 A and 160 μs for the maximum MRR and minimum WWR, whereas 45 μs pulse off-time and 6 m/min wire feed were the optimum settings that was obtained for MRR. Also,

for WWR the optimum settings were obtained at 40 μs pulse off-time and 10 m/min wire feed.
- Optimal results achieved through NSGA-II are in accordance with experimental outcomes having the maximum absolute percentage errors as 6.784% and 7.589% for MRR and WWR, respectively.

Declaration

References

1. Aggarwal V, Khangura SS, Garg RK (2015) Parametric modeling and optimization for wire electrical discharge machining of Inconel 718 using response surface methodology. Int J Adv Manuf Technol 79(1–4):31–47
2. Magabe R, Sharma N, Gupta K, Davim JP (2019) Modeling and optimization of Wire-EDM parameters for machining of Ni 55.8 Ti shape memory alloy using hybrid approach of Taguchi and NSGA-II. Int J Adv Manuf Technol 102(5–8):1703–1717
3. Kanagarajan D, Karthikeyan R, Palanikumar K, Davim JP (2008) Optimization of electrical discharge machining characteristics of WC/Co composites using non-dominated sorting genetic algorithm (NSGA-II). Int J Adv Manuf Technol 36(11–12):1124–1132
4. Eswaramoorthy SB, Shanmugham EP (2015) Optimal control parameters of machining in CNC wire-cut EDM for titanium. Int J Appl Sci Eng Res 4(1):102–121
5. Dambatta YS, Sayuti M, Sarhan AA, Ab Shukor HB, Binti Derahman NA, Manladan SM (2019) Prediction of specific grinding forces and surface roughness in machining of AL6061-T6 alloy using ANFIS technique. Ind Lubr Tribol 71:309–317
6. Sharma N, Khanna R, Gupta RD (2015) WEDM process variables investigation for HSLA by response surface methodology and genetic algorithm. Eng Sci Technol Int J 18(2):171–177
7. Mahapatra SS, Patnaik A (2006) Parametric optimization of wire electrical discharge machining (WEDM) process using Taguchi method. J Braz Soc Mech Sci Eng 28(4):422–429

8. Goyal A (2017) Investigation of material removal rate and surface roughness during wire electrical discharge machining (WEDM) of Inconel 625 super alloy by cryogenic treated tool electrode. J King Saud Univ Sci 29(4):528–535

9. Gauri SK, Chakraborty S (2010) A study on the performance of some multi-response optimisation methods for WEDM processes. Int J Adv Manuf Technol 49(1–4):155–166

10. Kuriachen B, Somashekhar KP, Mathew J (2015) Multiresponse optimization of micro-wire electrical discharge machining process. Int J Adv Manuf Technol 76(1–4):91–104

11. Manna A, Bhattacharyya B (2006) Taguchi and Gauss elimination method: a dual response approach for parametric optimization of CNC wire cut EDM of PRAlSiCMMC. Int J Adv Manuf Technol 28(1–2):67–75

12. Bobbili R, Madhu V, Gogia AK (2015) Modelling and analysis of material removal rate and surface roughness in wire-cut EDM of armour materials. Eng Sci Technol Int J 18(4):664–668

13. Majumder A (2013) Process parameter optimization during EDM of AISI 316 LN stainless steel by using fuzzy based multi-objective PSO. J Mech Sci Technol 27(7):2143–2151

14. Maji K, Pratihar DK (2011) Modeling of electrical discharge machining process using conventional regression analysis and genetic algorithms. J Mater Eng Perform 20(7):1121–1127

15. Pasam VK, Battula SB, Madar Valli P, Swapna M (2010) Optimizing surface finish in WEDM using the Taguchi parameter design method. J Braz Soc Mech Sci Eng 32(2):107–113

16. Goswami A, Kumar J (2014) Investigation of surface integrity, material removal rate and wire wear ratio for WEDM of Nimonic 80A alloy using GRA and Taguchi method. Eng Sci Technol Int J 17(4):173–184

17. Torres A, Puertas I, Luis CJ (2016) EDM machinability and surface roughness analysis of INCONEL 600 using graphite electrodes. Int J Adv Manuf Technol 84(9–12):2671–2688

18. Singh V, Bhandari R, Yadav VK (2017) An experimental investigation on machining parameters of AISI D2 steel using WEDM. Int J Adv Manuf Technol 93(1–4):203–214

19. Kumar SS, Uthayakumar M, Kumaran ST, Parameswaran P, Mohandas E, Kempulraj G, Babu BR, Natarajan SA (2015) Parametric optimization of wire electrical discharge machining on aluminium based composites through grey relational analysis. J Manuf Process 20:33–39

20. Yang RT, Tzeng CJ, Yang YK, Hsieh MH (2012) Optimization of wire electrical discharge machining process parameters for cutting tungsten. Int J Adv Manuf Technol 60(1–4):135–147

21. Yadav RN, Yadava V (2013) Multiobjective optimization of slotted electrical discharge abrasive grinding of metal matrix composite using artificial neural network and nondominated sorting genetic algorithm. Proc Inst Mech Eng Part B J Eng Manuf 227(10):1442–1452

22. Conde A, Arriandiaga A, Sanchez JA, Portillo E, Plaza S, Cabanes I (2018) High accuracy wire electrical discharge machining using artificial neural networks and optimization techniques. Robot Comput Integr Manuf 49:24–38

23. Mukhopadhyay A, Barman TK, Sahoo P, Davim JP (2019) Modeling and optimization of fractal dimension in wire electrical discharge machining of EN 31 steel using the ANN-GA approach. Materials 12(3):454

24. Shakeri S, Ghassemi A, Hassani M, Hajian A (2016) Investigation of material removal rate and surface roughness in wire electrical discharge machining process for cementation alloy steel using artificial neural network. Int J Adv Manuf Technol 82(1–4):549–557

25. Goyal A, Rahman HU, Ghani SAC (2020) Experimental investigation and optimisation of wire electrical discharge machining process parameters for Ni49Ti51 shape memory alloy. J King Saud Univ Eng Sci 33:129–135

26. Das PP, Diyaley S, Chakraborty S, Ghadai RK (2019) Multi-objective optimization of wire electro discharge machining (WEDM) process parameters using grey-fuzzy approach. Period Polytech Mech Eng 63(1):16–25

27. Vates UK, Singh NK, Singh RV (2016) Modelling and optimisation of wire electrical discharge machining process on D2 steel using ANN and RMSE approach. Int J Comput Mater Sci Surf Eng 6(3–4):161–185

28. Hasçalık A, Çaydaş U (2007) Electrical discharge machining of titanium alloy (Ti–6Al–4V). Appl Surf Sci 253(22):9007–9016

29. Javadi Y, Sadeghi S, Najafabadi MA (2014) Taguchi optimization and ultrasonic measurement of residual stresses in the friction stir welding. Mater Des 55:27–34

30. Ramamurthy A, Sivaramakrishnan R, Muthuramalingam T (2015) Taguchi-Grey computation methodology for optimum multiple performance measures on machining titanium alloy in WEDM process. Indian J Eng Mater Sci (IJEMS) 22:181–186

31. Sai T, Pathak VK, Srivastava AK (2020) Modeling and optimization of fused deposition modeling (FDM) process through printing PLA implants using adaptive neuro-fuzzy inference system (ANFIS) model and whale optimization algorithm. J Braz Soc Mech Sci Eng 42(12):1–19

32. Unune DR, Nirala CK, Mali HS (2018) ANN-NSGA-II dual approach for modeling and optimization in abrasive mixed electro discharge diamond grinding of Monel K-500. Eng Sci Technol Int J 21(3):322–329

33. Deb K, Pratap A, Agarwal S, Meyarivan TAMT (2002) A fast and elitist multiobjective genetic algorithm: NSGA-II. IEEE Trans Evol Comput 6(2):182–197

34. Huu PN, Tien LB, Duc QT, Van DP, Xuan CN, Van TN, Duc LN, Jamil M, Khan AM (2019) Multi-objective optimization of process parameter in EDM using low-frequency vibration of workpiece assigned for SKD61. Sādhanā 44(10):1–11